

Stochastic fluctuations in the rotation of the bacterial flagellar motor

Guanhua Yue(岳冠骅), Rongjing Zhang(张榕京), and Junhua Yuan(袁军华)
Citation: Chin. Phys. B, 2023, 32 (**6**): 068703. DOI: 10.1088/1674-1056/acc804
Journal homepage: http://cpb.iphy.ac.cn; http://iopscience.iop.org/cpb

What follows is a list of articles you may be interested in

Influence of matrix-metalloproteinase inhibitor on the interaction between cancer cells and matrigel

Teng Ye(叶腾), Fangfu Ye(叶方富), Feng Qiu(邱峰)
Chin. Phys. B, 2020, 29 (**6**): 068701. DOI: 10.1088/1674-1056/ab85c1

Influence of matrigel on the shape and dynamics of cancer cells

Teng Ye(叶腾), Feng Qiu(邱峰)
Chin. Phys. B, 2019, 28 (**10**): 108704. DOI: 10.1088/1674-1056/ab4275

Quantitative heterogeneity and subgroup classification based on motility of breast cancer cells

Ling Xiong(熊玲), Yanping Liu(刘艳平), Ruchuan Liu(刘如川), Wei Yuan(袁伟), Gao Wang(王高), Yi He(何益), Jianwei Shuai(帅建伟), Yang Jiao(焦阳), Xixiang Zhang(张溪祥), Weijing Han(韩伟静), Junle Qu(屈军乐), Liyu Liu(刘雳宇)
Chin. Phys. B, 2019, 28 (**10**): 108701. DOI: 10.1088/1674-1056/ab3af4

Diffusional inhomogeneity in cell cultures

Jia-Zheng Zhang(张佳政), Na Li(李娜), Wei Chen(陈唯)
Chin. Phys. B, 2018, 27 (**2**): 028705. DOI: 10.1088/1674-1056/27/2/028705

Stability of focal adhesion enhanced by its inner force fluctuation

Mao Zhi-Xiu (毛志秀), Chen Xiao-Feng (陈笑风), Chen Bin (陈彬)
Chin. Phys. B, 2015, 24 (**8**): 088702. DOI: 10.1088/1674-1056/24/8/088702

RAPID COMMUNICATION

Stochastic fluctuations in the rotation of the bacterial flagellar motor

Guanhua Yue(岳冠骅), Rongjing Zhang(张榕京)[†], and Junhua Yuan(袁军华)[‡]

Department of Physics, University of Science and Technology of China, Hefei 230026, *China*

(Received 1 February 2023; revised manuscript received 16 March 2023; accepted manuscript online 28 March 2023)

The bacterial flagellar motor is a nanometer-sized rotary motor that generates the torque to drive the rotation of the flagellar filament. The output torque is an important property of the motor. The motor rotation was usually monitored by attaching a μm-sized bead to a shortened flagellar filament, and the torque was extracted by calculating the torque due to the viscous drag of the medium on the bead rotation. We sought for an independent extraction of the torque from thermal fluctuation in the motor rotation using the fluctuation theorem (FT). However, we identified an overwhelming fluctuation beyond the thermal noise that precluded the use of FT. We further characterized the timescale and the amplitude of this fluctuation, finding that it was probably due to the stepping of the motor. The amplitude of torque fluctuation we characterized here provided new information on the torque-generating interaction potential curve.

Keywords: motor torque, bacterial motility, fluctuation theorem, viscous drag

PACS: 87.85.gj, 87.15.Ya, 87.17.Jj, 05.10.Gg **DOI:** 10.1088/1674-1056/acc804

1. Introduction

Flagellated bacteria, such as *Escherichia coli*, swim by rotating thin helical flagellar filaments, each driven at its base by a reversal rotary motor.[1] The flagellar motor is embedded in the cell envelope, and powered by a transmembrane proton flux.[2] The motor consists of two parts, a rotary part (rotor) and a set of torque-generating units (stators) around the rotor. The rotor comprises four ring structures (the cytoplasmic C-ring, the inner membrane-embedded MS-ring, the P-ring, and the L-ring), and along the center axis of the ring structures, a short rod across the peptidoglycan and the outer membrane, which connects via the flexible hook (approximately 55 nm long) to the long filament (up to 10 μm in length).[3–5] Each stator consists of five MotA and two MotB proteins that form two proton-conducting transmembrane channels.[6,7] Driven by a proton electrochemical potential difference across the inner membrane (the proton motive force, PMF), the protons flow through the channels and induce conformational changes of the stator that exert force on the C-ring of the rotor via electrostatic and steric interactions.[2,5] Each motor can contain up to 11 independently working stators, although normally in a wildtype cell, the number of stators is about 7 or 8 for a motor under high load.[8] The motor can rotate counterclockwise (CCW) or clockwise (CW), depending upon the conformation of the C-ring.[9]

The relationship between the motor torque and the motor angular speed is one of the most important characteristics of the motor, measuring how much torque the motor generates at different speeds (under different loads). As the speed increases (load decreases), the torque remains nearly constant up to an intermediate speed called the "knee speed", after which it falls rapidly to zero.[10–12] The near-constant motor torque at high loads was usually measured by attaching a μm-sized latex bead to the shortened filament, and extracting from the speed ω and viscous drag coefficient of bead rotation γ : $N = \gamma\omega$. As the bead rotates near the surfaces of a cell and the cover glass of the sample chamber, the contribution of the surface effect to γ is usually significant but difficult to estimate:[13] first, the main contribution of the surface effect is from the surface of the cell body, which is a cylindrical surface instead of a flat surface; second, the distance between the bead and the cell body is small and difficult to precisely measure.

In recent years, nonequilibrium statistical mechanics have been increasingly widely used in biological systems, such as Jarzynski's equality,[14] Crooks fluctuation theorem[15] and the fluctuation theorem (FT).[16] We sought to measure the motor torque at high loads independently with FT, which used the thermal fluctuation in the rotation of the bead, under the assumption that the motor torque is constant at high loads.[17] This was similar to that applied to measure the torque of the F_1-ATPase single molecule rotary motor.[18] Using FT to extract the torque eliminated the need to calculate γ, but the rotation of the motor needed to be measured with high spatiotemporal resolution using the bead assay, and with other noises besides the thermal noise well controlled and removed, which we carried out below.

We performed the experiments for motor rotation under high load and analyzed the fluctuations of the rotation. However, we found that there exists an extra ultrafast fluctuation that overwhelms the thermal fluctuation. By eliminating var-

[†]Corresponding author. E-mail: rjzhang@ustc.edu.cn
[‡]Corresponding author. E-mail: jhyuan@ustc.edu.cn

© 2023 Chinese Physical Society and IOP Publishing Ltd

ious types of experimental noises,[19,20] we characterized the timescale and amplitude of this unknown fluctuation, finding that it was probably due to stepping in the motor rotation.[21,22]

2. Experimental materials and methods

2.1. Strains and plasmids

The strain we used is JY21 (*motA448* Δ*fliC* Δ*cheY*), which was derived from *E. coli* K12 strain RP437.[23] The plasmid pKAF131 constitutively expresses the sticky filament FliC^{st}, and the plasmid pTrc99aMotA expresses wildtype MotA under control of an IPTG-inducible promoter.[24]

2.2. Cell culture

Bacteria were grown at 33 °C in 10 ml of T-broth (1% tryptone and 0.5% NaCl) with appropriate antibiotics (ampicillin (100 mg/ml) and chloramphenicol (25 mg/ml)) and the inducer IPTG at the appropriate final concentrations: 0 μM, 10 μM, 20 μM, 50 μM, and 100 μM. Cells were grown to an OD_{600} (optical density at 600 nm) of between 0.45 and 0.50, and 1 ml of the grown culture was harvested by centrifugation at 4000 × *g* for 2 min, washed twice with 1 ml motility medium [10 mM potassium phosphate, 0.1 mM EDTA, 1 mM methionine, and 10 mM lactic acid, at pH 7.0], and resuspended in 1 ml of this medium.

2.3. Bead assay

We truncated the flagella by passing 1 ml of the washed cell suspension between two syringes equipped with 23-gauge needles and connected by 7-cm-long polyethylene tubing (0.58 mm inside diameter, No. 427411; Becton Dickinson) for 60 to 70 times. The sheared cell suspension was centrifuged and resuspended in 0.7 ml of motility medium.

To measure the motor speed trace, we constructed a sample chamber with two pieces of double-sided tape spaced between the coverslip and a glass slide. The glass coverslip was coated with poly-L-lysine by adding 40 μl poly-L-lysine (0.01%, P4707; Sigma, St. Louis, MO), allowing to stand for 5 min, and then rinsing with 100 μl motility medium. 40 μl of the sheared cell suspension was added to the coverslip, allowed to stand for 10 min, and then rinsed with 40 μl of 40× diluted 0.75-μm-diameter or 15× diluted 1.5-μm-diameter polystyrene latex bead solutions (No. 07306; Polysciences) to attach the beads to the sheared flagellar stubs. After incubating for 3 min, the chamber was rinsed with 200 μl motility medium with various Ficoll concentrations (0 or 5% or 15% w/v). The chamber was then sealed with vacuum grease. This procedure allowed sticking the cell to the coverslip and attaching a bead to the truncated flagellar filament so that the bead rotation could be followed. We used a Nikon Ti-E phase-contrast microscope (Nikon, Melville, NY) with an objective magnification of 40× to observe the bead, and the images were recorded by an sCMOS camera (OLCA-Flash4.0 V2, Hamamastu Photonics, Hamamatsu, Japan) at frame rates ranging from 1500–2500 Hz with a reduced region of interest that covered selected trajectories of beads. Occasionally, some beads were stuck to the coverslip instead of attaching to the filament stubs. The images of some of those stuck beads were also recorded to correct for the drift of the sample stage.

2.4. Data analysis

Data analysis was carried out using custom scripts in MATLAB (MathWorks). For each frame, the positions of both the stuck bead and the rotating bead were calculated as the averaged pixel position weighted by the intensity of the pixels, and then the position of the stuck bead was subtracted from the position of the rotating bead to eliminate the long-term drift of the sample stage. In the conventional bead assay, the effect due to the drift of the sample stage was usually not corrected, or crudely corrected by dividing the time traces of bead trajectory into subsections and shifting the trajectory center of each subsection to match each other. Here, we used the dual-bead method to precisely correct the drift of the sample stage. The bead positions were converted into angular positions relative to the center of the bead rotating trajectory by using the atan2 function in MATLAB, and then the angular speeds were calculated from changes in the angular positions.

We took care to control the number of stators in the motor to eliminate the possible effect of torque change due to changes in the number of stators. The stators of the motor bind to and unbind from the rotor stochastically on a timescale of 1 min. At high load, the motor torque is proportional to the stator number.[13,24] Thus, the steady-state speed trace of the motor showed step-like fluctuations corresponding to changes in the number of bound stators.[24] For each rotating motor, we recorded for 20 min to ensure that binding and unbinding of the stators occurred enough times so that we could analyze the speed time series with a step-finding algorithm.

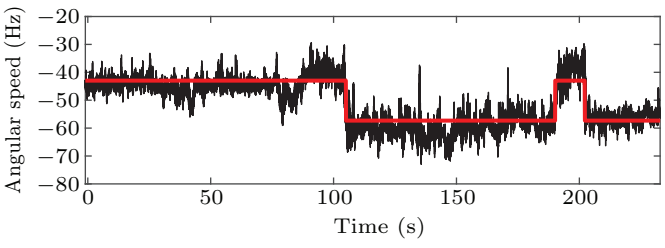


Fig. 1. Typical trace of motor angular speeds at steady state. The black line is the speed time trace. The red lines are the average speeds found by the step-finding algorithm.

We first used the Chug–Kennedy filtering algorithm (C-K filter) to filter the angular speed trace.[25] The analytical window used in the filter was [0.1 s, 0.5 s, 1.0 s] for experiments with 0.75-μm-diameter beads and [0.5 s, 2.5 s, 5.0 s] for experiments with 1.5-μm-diameter beads. We then used a step-finding algorithm as described previously to identify the speed

steps,[24,26] and the number of stators in each segment was calculated as the average speed of this segment divided by the mean step size. A typical trace of motor angular speeds with identified steps is shown in Fig. 1. After identifying the segments, each with stable numbers of stators, we divided each segment into small 5 s-long sections, and selected the sections during which the motor rotated stably. The averaged variance in angular displacement $\Delta\phi$ during a time interval of Δt, $\sigma_\phi^2(\Delta t)$, of these sections was calculated.

3. Results

3.1. Measuring the motor rotation

To study the fluctuation in motor rotation more precisely, we chose the *E. coli* strain JY21, which rotates only in the CCW direction. JY21 also carries a null mutation of the stator gene *motA* and a null mutation of the filament gene *fliC*. JY21 was transformed with the plasmid pKAF131 that expressed the sticky *fliC* allele to allow attaching a latex bead to the filament, and the plasmid pTrc99aMotA that expressed the wild-type MotA under control of an IPTG-inducible promoter to allow controlling the number of stators in a motor.[27]

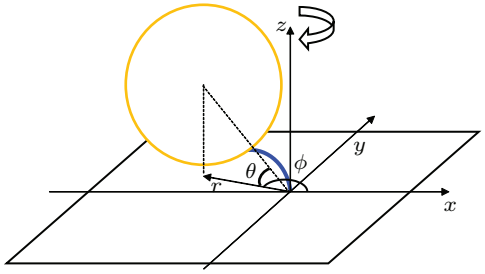


Fig. 2. Schematic diagram of attached bead rotation. The blue line denotes the shortened filament stub, the yellow circle denotes the latex bead, the *xy* plane is parallel to the plane of rotation, θ is the inclination angle, and r and ϕ are the radius and angle of rotation, respectively. The cell body, which lies at the end of the filament stub, is omitted from the diagram.

For the rotation of a bead shown schematically in Fig. 2 with constant torque N and frictional drag coefficient γ, the time evolution of the rotation angle $\phi(t)$ is described by the Langevin equation

$$\gamma\frac{\mathrm{d}\phi(t)}{\mathrm{d}t} = N + \xi, \tag{1}$$

where $\xi(t) = \sqrt{2\gamma k_\mathrm{B}T}\Gamma(t)$ is a random torque that represents the effects of thermal fluctuation, k_B is the Boltzmann constant, T is the room temperature ($T = 296$ K), and $\Gamma(t)$ is Gaussian white noise whose autocorrelation function is the delta-function: $\langle\Gamma(t)\Gamma(t')\rangle = \delta(t-t')$. Assuming that N is constant, FT has the following form for torque measurement:[18]

$$\ln\left(\frac{P(\Delta\phi)}{P(-\Delta\phi)}\right) = N\frac{\Delta\phi}{k_\mathrm{B}T}, \tag{2}$$

where $P(\Delta\phi)$ is the probability distribution of the angular displacement $\Delta\phi$ during a time interval of Δt, $\Delta\phi = \phi(t+\Delta t) - \phi(t)$.

We chose 0.75-μm-diameter latex beads and performed the bead assay. Since the stator can bind to and unbind from the rotor stochastically (on a timescale of 1 min), we used JY21 with pTrc99aMotA to control the number of stators by using different concentrations of the inducer IPTG.[24] To accurately eliminate the low-frequency drift of the sample stage, we captured the rotating bead and a stable bead stuck to the cover glass of the sample chamber simultaneously (Fig. 3(a)), and computed the corrected coordinates (x, y) of the center of the rotating bead by subtracting the coordinates of the stable bead. An example of the corrected trajectory of the bead rotation is shown in Fig. 3(b). We chose rotation trace sections during which the motor rotated stably for at least 5 s for further analysis (Fig. 3(c)), and the angular speed was calculated from changes in the bead angular positions.

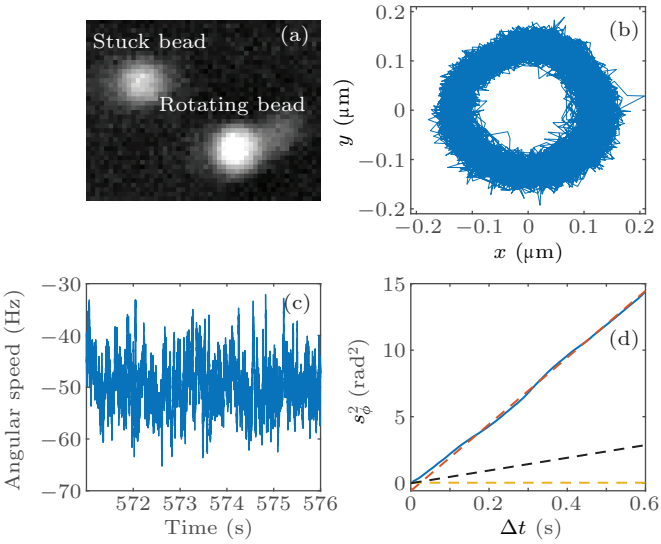


Fig. 3. (a) An example image of a rotating bead (right) and a stable bead stuck to the cover glass (left) captured by the camera. (b) The rotation trajectory of the rotating bead for 5 s, which was corrected for the drift of the sample stage and with the trajectory center moved to (0, 0). (c) The calculated angular speed of this rotation trace section, which has been filtered by running average with a window size of 0.02 s. (d) $\sigma_\phi^2(\Delta t)$ as a function of Δt. The blue solid line is the experimental data, the red dashed line is the linear fitting of the experimental data in the time range of 0.1 s to 0.5 s, the black dashed line is $\sigma_\phi^2(\Delta t) = 2D_0\Delta t$, which is induced by the thermal noise with $D_0 = k_\mathrm{B}T/\gamma$, and the yellow dashed line near the x-axis is the $\sigma_\phi^2(\Delta t)$ induced by the bending flexibility of the hook and the camera detection noise.

When the motor rotates under high load, the torque is usually thought to be constant, and the fluctuation in the bead speeds is due to thermal noise,[17] so that the motor rotation satisfies Eq. (1) and the motor torque can be extracted using FT (Eq. (2)). However, when we tried using Eq. (2) to compute the torque N, the resulting N was significantly smaller than the torque extracted directly from $N = \gamma\omega$ as normally done previously with

$$\gamma = \eta\left(8\pi a^3 + 6\pi a r^2\right),$$

where a and r are the bead radius and the trajectory radius, respectively, and η is the viscosity of the medium.[12] The extracted N using FT is about 40 pN·nm per stator, whereas that from $N = \gamma\omega$ is about 175 pN·nm (see Fig. S1 and details in the supplemental material). This suggested that there existed other types of noise in the motor rotation, which were much larger than the thermal noise. Note that in the above formula for γ where the surface effect was not included, the first term corresponded to the drag coefficient of a sphere rotating about an axis through its center, and the second term came from the fact that the rotational axis was off the center by a distance of r.

To study noises beyond the thermal noise, we focused on the variance of $\Delta\phi$, $\sigma_\phi^2(\Delta t) = \mathrm{Var}(\Delta\phi(\Delta t)) = \langle(\phi(t+\Delta t) - \phi(t)^2\rangle - \langle(\phi(t+\Delta t) - \phi(t))\rangle^2$, with different values of the time interval Δt.

The measured distribution $P(\Delta\phi)$ can be well fit with a Gaussian function (Fig. S2)

$$P(\Delta\phi) = \frac{1}{\sqrt{2\pi\sigma^2}} \exp\left(-\frac{(\Delta\phi - \mu)^2}{2\sigma^2}\right), \tag{3}$$

where the parameters σ^2 and μ are the variance and the mean of $\Delta\phi$, respectively. For thermal noise, $\sigma_\phi^2(\Delta t) = \sigma^2 = 2k_\mathrm{B}T\Delta t/\gamma$, and $\mu = N\Delta t/\gamma$. We could see that if we substituted Eq. (3) with the expressions of σ^2 and μ for thermal noise into Eq. (2), Eq. (2) was automatically satisfied. Therefore, the magnitude of $\sigma_\phi^2(\Delta t)$ determines the value of N extracted using FT, with larger $\sigma_\phi^2(\Delta t)$ leading to smaller N. Comparing the experimentally measured $\sigma_\phi^2(\Delta t)$ with that induced by the thermal noise $2k_\mathrm{B}T\Delta t/\gamma$ could characterize the extra noise beyond the thermal noise. $\sigma_\phi^2(\Delta t)$ computed from the experimental data (blue solid line in Fig. 3(d)) was significantly larger than $2k_\mathrm{B}T\Delta t/\gamma$ (black dashed line in Fig. 3(d)), suggesting a large amplitude of extra noise.

3.2. Other sources of noise

Two possible sources of fluctuations included the precision in detecting the bead position and the tangential flexing of the hook due to the hook bending compliance (the filament is rigid). Assuming isotropic bending of the hook, the tangential flexing is the same as the radial flexing of the hook. The noise due to detection precision and hook flexing could be extracted from the radial fluctuation of the bead trajectory. According to a recent work,[20] from the radial fluctuation of the bead positions shown in Fig. 3(d), and the characteristic time of hook bending, we could extract the average angle of inclination θ as shown in Fig. 2, and then both noises due to detection precision and hook flexing (see supplemental material). The amplitude of the noise due to hook flexing is at a similar level to that of the detection noise, and $\sigma_\phi^2(\Delta t)$ due to both noises is shown in Fig. 3(d) as the yellow dashed line, which is a very minor contribution to the experimentally measured $\sigma_\phi^2(\Delta t)$.

We also considered the noise from the relative angular displacement between the bead and rotor due to torsional compliance of the hook (see supplemental material).[19] This type of noise is extremely small and can be neglected, similar to the condition in F_1-ATPase.[18]

The amplitude of all three types of noises mentioned above is small when Δt is relatively large. Thus, they cannot be the major source of the difference between the experimentally measured $\sigma_\phi^2(\Delta t)$ and $2k_\mathrm{B}T\Delta t/\gamma$ due to the thermal noise for relatively large Δt in Fig. 3(d). Furthermore, we can see that the experimentally measured $\sigma_\phi^2(\Delta t)$ scales approximately linearly with Δt:

$$\sigma_\phi^2(\Delta t) \approx 2D_\mathrm{tot}\Delta t,$$

where D_tot is the total diffusion coefficient.

The other possible contribution to the difference between the experimentally measured $\sigma_\phi^2(\Delta t)$ and $2k_\mathrm{B}T\Delta t/\gamma$ is the fluctuation of the motor torque, which we sought to characterize further below.

3.3. Fluctuation of the motor torque

Fluctuation of the motor torque around the average torque N_0 can be described using the Langevin equation

$$\frac{\mathrm{d}N(t)}{\mathrm{d}t} + \frac{1}{\tau_N}(N(t) - N_0) = \sqrt{2A_\mathrm{torque}}\Gamma(t), \tag{4}$$

$$\frac{\mathrm{d}\phi(t)}{\mathrm{d}t} = \frac{1}{\gamma}N, \tag{5}$$

where τ_N is the relaxation time in the torque fluctuation, and the constant A_torque characterizes the amplitude of the Gaussian white noise, with $\sigma^2(N) = A_\mathrm{torque}\cdot\tau_N$.

Equations (4) and (5) have the same mathematical form as the free diffusion of a massive particle (see supplemental material), so $\sigma_\phi^2(\Delta t)$ due to fluctuation of the motor torque is

$$\sigma_\phi^2(\Delta t) = 2D_N\Delta t - 2D_N\tau_N\left(1 - \mathrm{e}^{-\frac{\Delta t}{\tau_N}}\right),$$

where D_N is the contribution to the diffusion coefficient from fluctuation of the motor torque, with $D_N\cdot\gamma^2 = A_\mathrm{torque}\cdot\tau_N^2$ such that $\sigma^2(N) = D_N\cdot\gamma^2/\tau_N$.

For large Δt, and combined with the variance due to thermal noise, we have

$$\begin{aligned}\sigma_\phi^2(\Delta t) &\approx 2D_N(\Delta t - \tau_N) + 2\frac{k_\mathrm{B}T}{\gamma}\Delta t \\ &= 2D_\mathrm{tot}\Delta t - 2D_N\tau_N,\end{aligned} \tag{6}$$

where $D_\mathrm{tot} = D_N + D_0$ with $D_0 = k_\mathrm{B}T/\gamma$.

We subtracted the three types of noises mentioned above (the noises due to detection precision, hook flexing, and relative angular displacement between the bead and rotor) from the experimental data, and the remaining $\sigma_\phi^2(\Delta t)$ should only contain the thermal noise and the fluctuation of the motor torque. We select the Δt range of 0.1 s to 0.5 s to fit the linear

function Eq. (6). We choose 0.1 s as the lower limit because the characteristic time of the fluctuation due to the hook flexing can be up to ~ 0.01 s when the stator number is 1.[20] From the linear fitting with Eq. (6), $D_{\rm tot}$ and thus D_N could be extracted from the slope, and then τ_N could be extracted from the intercept at $\Delta t = 0$ s. For example, for the data shown in Fig. 3(d), we fit it in the Δt range of 0.1 s to 0.5 s with Eq. (6), resulting in a slope ($2D_{\rm tot}$) of 25.07 rad$^2 \cdot$ s^{-1} and an intercept ($-2D_N\tau_N$) at $\Delta t = 0$ s of -0.580 rad^2. The value of D_0 can be obtained from the value of γ, leading to $2D_0 = 4.77$ rad$^2 \cdot$ s^{-1}. Thus, the value of D_N can be obtained from the difference between $D_{\rm tot}$ and D_0, leading to a value of 10.15 rad$^2 \cdot$ s^{-1}, and the value of τ_N can be obtained from the fitted intercept and the value of D_N, leading to a value of 0.0304 s.

For different stator numbers, we extracted the values of D_N and τ_N, as shown in Fig. 4.

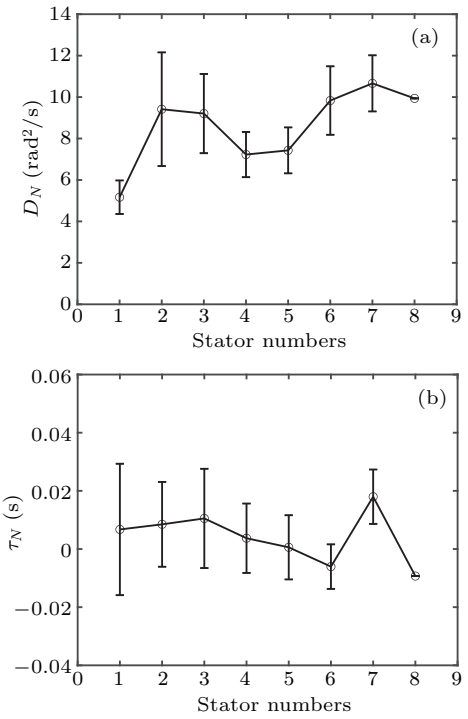


Fig. 4. The extracted D_N and τ_N at different stator numbers. Error bar shows the standard error of the mean (SEM). For stator numbers of 1 to 8, the numbers of trace segments we collected were 4, 13, 20, 24, 13, 5, 3, and 1, respectively. Thus, there is no error bar for stator number of 8.

The numbers of trace segments we collected for stator numbers from 1 to 8 were 4, 13, 20, 24, 13, 5, 3, and 1, respectively, with an average stator number of 3.73±0.16. D_N for different stator numbers are relatively constant, with $D_N = 8.29 \pm 0.39$ rad^2/s for all the data. The timescale τ_N in the torque fluctuation is extremely small, with very large uncertainty in the extracted value of τ_N. $\tau_N = 0.0055 \pm 0.0027$ s for all the data. Due to the large uncertainty in measuring τ_N, we could quote an upper limit of it: $\tau_N < 0.0082$ s. This suggested an extremely fast fluctuation of the motor torque, consistent with the timescale of motor stepping, which was around $1/(n \times \omega)$, where $n = 26$ or 34 is the number of steps per revolution. The amplitude of the torque fluctuation was calculated to be $\sigma(N) = \sqrt{D_N \cdot \gamma^2/\tau_N} = 68.99 \pm 24.04$ pN·nm, with a relative fluctuation of $\sigma(N)/N = (13.0 \pm 4.6)\,\%$. Note that in Fig. 4, some of the extracted values of τ_N were unphysically negative: for some of the data of $\sigma_\phi^2(\Delta t)$ versus Δt (Fig. 3(d)), the fitted value of the intercept ($-2D_N\tau_N$) could be positive due to experimental noises, and this would lead to an unphysical negative τ_N as the value of the extracted D_N was always positive due to the large amplitude of torque fluctuation. The fact that some of the extracted τ_N values were negative was because of the extremely small value of τ_N and the large experimental uncertainty in extracting τ_N.

3.4. The relative contributions of torque fluctuation and thermal noise

We noticed that for different loads γ, the relative contributions of the two types of noise are different. As the amplitude of torque fluctuation is relatively constant with γ under high loads, $\gamma^2 \cdot D_N$ is constant with γ, which means $D_N \propto \gamma^{-2}$. The contribution from the thermal noise D_0 scales with $1/\gamma$. Thus the ratio of $D_{\rm tot}/D_0$ is

$$\frac{D_{\rm tot}}{D_0} = 1 + \frac{D_N}{D_0} = 1 + \frac{C}{\gamma},$$

where C is a constant. Thus, if we plot the values of $D_{\rm tot}/D_0$ at different values of $1/\gamma$, it should be a linear function, with a y intersect of 1. To verify this, we performed experiments by using 1.5-μm-diameter beads and changing the medium viscosity with Ficoll concentrations of 0%, 5% and 15%. The fluctuation of torque at large γ was smaller, so we could select longer trace segments, each of 30 s, and used a Δt range of 2–3 s to fit a linear function to extract $D_{\rm tot}$. As shown in Fig. 5, the data can be fit with a linear function, resulting in a y intersect of 1.17 ± 0.77. This was consistent with our prediction. Thus, the contribution from the thermal noise will dominate at sufficiently high loads, suggesting that we may be able to use FT to estimate the motor torque at extremely high loads.

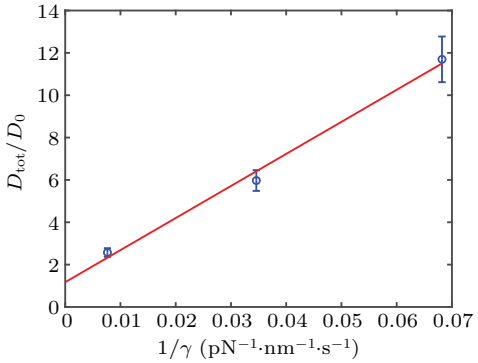


Fig. 5. The $D_{\rm tot}/D_0$ as a function of $1/\gamma$. Blue circles denote the values of $D_{\rm tot}/D_0$ for motors under loads of 1.5-μm-diameter bead and in medium with Ficoll concentrations of 15% ($n = 21$), 5% ($n = 24$) and 0% ($n = 25$) from left to right, respectively. Error bar is SEM. The red line is the linear fitting.

4. Discussion

The fluctuation theorem could provide an independent extraction of the motor torque at high loads. Here, we sought to perform this extraction, but discovered a large extra fluctuation in the motor torque that precluded it. We characterized the timescale and amplitude of this fluctuation. The timescale was extremely small, such that the uncertainty in measuring the timescale was large. We found an average timescale of 0.0055 ± 0.0027 s. Considering the large uncertainty in measuring the timescale, we could quote an upper limit of it: $\tau_N < 0.0082$ s. This was consistent with the timescale of motor stepping, which was around $1/(n \times \omega)$, where $n = 26$ or 34 is the number of steps per revolution. Therefore, the fluctuation of motor torque was probably due to motor stepping. The relative fluctuation of the motor torque was $(13.0 \pm 4.6)\%$. To measure the timescale of torque fluctuation more precisely, we could probably use a hook mutation that makes a more rigid hook[28] in the future.

The bacterial flagellar motor is a stepping rotary motor, with each stator stepping on the ring of FliG subunits to rotate the rotor. As the stepping timescale of the motor is extremely small, the motor stepping behavior is difficult to observe experimentally,[21,22] not to mention the characteristics of the motor stepping behavior. Due to technical difficulties, no experiments have attempted to measure the detailed properties of the stator–rotor interaction. Our measured amplitude of the fluctuation in the motor torque provided new information on the shape of the stator–rotor interaction potential curve.[17,29]

We also found that thermal noise would be dominant over the torque fluctuation at extremely high loads. This suggested that it may be feasible to estimate the motor torque using FT at extremely high loads.

The F1-ATPase rotary motor is also a stepping motor; thus, similar torque fluctuations caused by stepping are unavoidable. Nevertheless, it is interesting that FT could be used to extract its torque.[18] At high ATP concentrations, the rotation of F1-ATPase appears smooth with a small dwell time for each step (about 1 ms), much smaller than the response time of the probe (a μm-sized bead, corresponding to an extremely high load for the F1-ATPase motor). Thus, this is similar to the case we discussed above: the thermal noise would be dominant over the torque fluctuation at extremely high loads, thereby making it feasible to estimate the torque using FT.

Acknowledgements

Project supported by the National Natural Science Foundation of China (Grant Nos. 11925406 and 12090053) and the National Key R&D Program of China (Grant No. 2019YFA0709303).

References

[1] Berg H C 2003 *Annu. Rev. Biochem.* **72** 19
[2] Blair D F 2003 *FEBS Lett.* **545** 86
[3] Paul K, Gonzalez-Bonet G, Bilwes A M, Crane B R and Blair D 2011 *EMBO J.* **30** 2962
[4] Kim E A, Panushka J, Meyer T, Carlisle R, Baker S, Ide N, Lynch M, Crane B R and Blair D F 2017 *J. Mol. Biol.* **429** 1305
[5] Gabel C V and Berg H C 2003 *Proc. Natl. Acad. Sci. USA* **100** 8748
[6] Santiveri M, Roa-Eguiara A, Kuhne C, Wadhwa N, Hu H, Berg H C, Erhardt M and Taylor N M I 2020 *Cell* **183** 1
[7] Deme J C, Johnson S, Vickery O, Muellbauer A, Monkhouse H, Griffiths T, James R H, Berks B, Coulton J W, Stansfeld P J and Lea S M 2020 *Nat. Microbiol.* **5** 1553
[8] Reid S W, Leake M C, Chandler J H, Lo C, Armitage J P and Berry R M 2006 *Proc. Natl. Acad. Sci. USA* **103** 8066
[9] Sarkar M K, Paul K and Blair D 2010 *Proc. Natl. Acad. Sci. USA* **107** 9370
[10] Chen X and Berg H C 2000 *Biophys. J.* **78** 1036
[11] Ryu W S, Berry R M and Berg H C 2000 *Nature* **403** 444
[12] Yuan J, Fahrner K A, Turner L and Berg H C 2010 *Proc. Natl. Acad. Sci. USA* **107** 12846
[13] Wang B, Yue G H, Zhang R J and Yuan J H 2022 *mBio* **13** e00782-22
[14] Liphardt J, Dumont S, Smith S B, Tinoco I and Bustamante C 2002 *Science* **296** 1832
[15] Cetiner U, Raz O, Sukharev S and Jarzynski C 2020 *Phys. Rev. Lett.* **124** 228101
[16] Hayashi K, Hasegawa S, Sagawa T, Tasaki S and Niwa S 2018 *Phys. Chem. Chem. Phys.* **20** 3403
[17] Meacci G and Tu Y 2009 *Proc. Natl. Acad. Sci. USA* **106** 3746
[18] Hayashi K, Ueno H, Iino R and Noji H 2010 *Phys. Rev. Lett.* **104** 218103
[19] Wang R, Chen Q, Zhang R and Yuan J 2020 *Biophys. J.* **118** 2718
[20] Nord A L, Biquet-Bisquert A, Abkarian M, Pigaglio T, Seduk F, Magalon A and Pedaci F 2022 *Nat. Commun.* **13** 2925
[21] Sowa Y, Rowe A D, Leake M C, Yakushi T, Homma M, Ishijima A and Berry R M 2005 *Nature* **437** 916
[22] Mora T, Yu H, Sowa Y and Wingreen N S 2009 *PLoS Comput. Biol.* **5** e1000540
[23] Parkinson J S 1978 *J. Bacteriol.* **135** 45
[24] Shi H, Ma S, Zhang R and Yuan J 2019 *Sci. Adv.* **5** eaau6885
[25] Chung S H and Kennedy R A 1991 *J. Neurosci. Methods* **40** 71
[26] Lele P P, Hosu B G and Berg H C 2013 *Proc. Natl. Acad. Sci. USA* **110** 11839
[27] Yuan J and Berg H 2008 *Proc. Natl. Acad. Sci. USA* **105** 1182
[28] Nakamura S, Hanaizumi Y, Morimoto Y V, Inoue Y, Erhardt M, Minamino T and Namba K 2020 *Mol. Microbiol.* **113** 755
[29] Tu Y and Cao Y 2018 *Phys. Rev. E* **97** 022403